

Calcium Phosphate Cement Composed of Hydroxyapatite Modified Silica and Polyuegenol as a Bone Filler Material

Tri Windarti^{1*}, Nor Basid Adiwibawa Prasetya¹, Ngadiwiyana Ngadiwiyana¹, and Limpat Nulandaya^{2,3}

¹Department of Chemistry, Faculty of Science and Mathematics, Universitas Diponegoro, Jl. Prof. Soedharto SH, Tembalang, Semarang 50275, Indonesia

²Center for Progressive Materials-Technology and Innovation Park, University of Pavol Jozef Šafárik, 04001 Košice, Slovakia

³Institute of Experimental Physics, Slovak Academy of Sciences, Watsonova 47, 04001 Košice, Slovakia

* **Corresponding author:**

email: tri.windarti@lecturer.undip.ac.id

Received: December 16, 2022

Accepted: March 10, 2023

DOI: 10.22146/ijc.80298

Abstract: A composite of hydroxyapatite modified silica (HAsiO₂) and 10% (w/w) polyuegenol (PE) was synthesized to produce a calcium phosphate cement with antibacterial activity. The compatibility of the composite (HAsiO₂_PE) with bone filler requirements was determined due to its crystal, surface, antibacterial, and cytocompatibility properties. The results showed that compositing HAsiO₂ and PE did not affect HA's chemical and crystal properties. The presence of PE changed HAsiO₂ morphology to be coarser and denser than before composited. PE tends to agglomerate but does not affect the hydrophilicity of HAsiO₂. The presence of PE increased the surface area and total pore volume but lowered the average pore size. Different from pure PE, the composite of HAsiO₂_PE that contains of 10% PE has higher antibacterial activity toward *Escherichia coli* than *Staphylococcus aureus*. The composite is biocompatible because the cytotoxicity test toward pre-osteoblast cells resulted in an IC₅₀ of 2092 µg/mL. Thus, due to its chemical, surface, antibacterial, and cytocompatibility properties, the HAsiO₂_PE composite can be recommended as a bone filler material.

Keywords: antibacterial; bone; calcium phosphate cement; hydroxyapatite; polyuegenol

■ INTRODUCTION

The material used in orthopedic surgery affects its susceptibility to infection. Implants provide a significant risk of infection since they are regarded as foreign bodies in the body [1-2]. On the other hand, tissue opening during surgery is susceptible to bacterial infection [3]. Osteomyelitis is an inflammation of the bone that is often caused by a bacterial infection. More than 50% of these infections are caused by *Staphylococcus aureus* bacteria, where 28% of them are resistant to methicillin [4]. *Staphylococcus* species made up approximately 36.88% of hip joint surgeries [5]. The problem of infection caused by the rejection of implants can be overcome by using materials that are biocompatible and have strong bioactivity. Hydroxyapatite (HA, Ca₁₀(PO₄)₆(OH)₂) is a calcium phosphate that fulfills these criteria. Moreover, HA can be produced into a paste to be used as an

injectable calcium phosphate cement (CPC) [6]. The surface morphology and mechanical strength of HA are the determining factors for successful implantation. HA must be combined with other materials, such as silica (SiO₂), to increase its mechanical strength because of its fragility [7-10]. HA, which is composited with SiO₂ from rice husk, shows that HA covers the surface of the composite. Therefore, the biocompatibility and bioactivity properties of HA can be preserved [11].

There have been several attempts to add antibacterial properties to HA, including by compositing with a polymer. The polymers already used are chitosan [12], carboxylated chitosan [13], and γ -polyglutamic acid [14]. As is the basis for selecting the main material for CPC, the selection of an antibacterial agent must also consider its biocompatibility properties. For this reason, polyuegenol (PE) is an alternative polymer that meets

these criteria. PE is the result of the polymerization of eugenol monomers. Eugenol has so far been applied as an antibacterial agent in dental treatment. Eugenol can be isolated from clove oil, nutmeg oil, and cinnamon bark. Eugenol's antibacterial activity was included in the "moderate-strong" level, where eugenol inhibited the growth of the tested pathogens, such as *Escherichia coli* and *S. aureus* [15-16]. Eugenol polymerization into PE is expected to produce antibacterial properties that can last long term. The antibacterial activity appears due to the release of eugenol as a result of the depolymerization of PE in a physiological environment. Several studies have shown that eugenol and its derivatives still exhibit antibacterial activity when encapsulated or combined with polymers such as poly(lactic acid)/gelatin [17], poly(ϵ -caprolactone)/gelatin [15], resorcinol diglycidyl ether [16], dopamine methacrylamide [18], poly(3-hydroxybutyrate-co-3-hydroxyvalerate) [19] and poly(eugenol-co-methylmethacrylate)/polypropylene [20]. A composite of HA-modified SiO₂ (HASiO₂) and PE (HASiO₂_PE) is expected to produce CPC with good antibacterial properties that can last a long time in the bone.

In this study, the HASiO₂ was synthesized in situ by the sol-gel method using cetyltrimethylammonium bromide (CTAB) surfactant as a morphology-directing agent [21-22]. PE was synthesized by polymerization of eugenol using BF₃ catalyst [10-12]. Both were used to make CPC by mixing with 2.5% Na₂HPO₄ solution in a ratio of 1:1 (w/v). The final cement was then characterized to ascertain its crystal parameters, surface characteristics, antibacterial activity, and cytotoxicity. CPC is expected to maintain the superior properties of HA as a bone implant so that, at the end, the transformation of the implant into living tissue can occur. In other words, the addition of antibacterial properties to CPC must be capable to accommodate the process of implant deformation and bone tissue formation by the activity of osteoclasts and osteoblasts cells [23].

■ EXPERIMENTAL SECTION

Materials

The Chemicals used for the synthesis of HASiO₂ were Ca(NO₃)₂·4H₂O (Merck), KH₂PO₄ (Merck), NH₄OH

(Merck), SiO₂ (Merck), and CTAB (Sigma Aldrich). For the synthesis of PE, eugenol (Merck), chloroform (Merck), anhydrous Na₂SO₄ (Merck), and BF₃ in diethyl ether were used. Materials for the production of CPC are synthesized HASiO₂ and PE as the powder component and Na₂HPO₄ (Merck). For the antibacterial test, DMSO (Merck), *E. coli* (gram-negative), and *S. aureus* (gram-positive) bacteria were used. While for the cytotoxicity test, pre-osteoblast MC3T3E1 cells, MEM- α media (Gibco), 10% FBS (Sigma Aldrich), 2% Pen-Strep (Gibco), Fungizone 0.5% (Gibco), 0.5 mg/mL MTT (Biobasic), DMSO (Merck) were used.

Procedure

Preparation of HASiO₂

The synthesis of hydroxyapatite-modified silica was conducted according to the previous work [11]. A 50 mL of a solution that contained Ca(NO₃)₂·4H₂O 1.2 M, SiO₂ 0.048 M, and CTAB (0.045 mmol) was slowly added by 50 mL of a solution that contained KH₂PO₄ 1 M and CTAB (0.045 mmol). The mixture was then added 15 mL of 32% NH₄OH to obtain a pH higher than 9 and stirred for 1 h. The mixture was then aged for 24 h at room temperature. The precipitate formed was washed with aquabidest until neutral and then dried in an electric oven at 50 °C for 48 h. The result was then calcined at 600 °C for 2 h in the air atmosphere. Then the product was ground and sieved by 200 mesh sieve. The obtained powder was called HASiO₂ sample.

Synthesis of PE

PE was obtained by adding chloroform solution to a three-neck flask containing eugenol (5.8 g, 35 mmol). During the polymerization process, the system was fed with nitrogen gas at room temperature while adding BF₃ in diethyl ether (1 mL) dropwise. Polymerization was carried out overnight, and the reaction was stopped by adding 1 mL of methanol. The polymerization results were dissolved in diethyl ether and then washed using distilled water until a neutral pH was reached. The organic layer was then dried by adding anhydrous Na₂SO₄. The solvent was evaporated with a rotary evaporator, and the PE residue was dried in a desiccator before being used.

Synthesis of HASiO₂_PE Composite

HASiO₂ and PE powder with a ratio of 9:1 (w/w) are used as the powder component, and 2.5% Na₂HPO₄ solution as a liquid component. CPC was made with a liquid:powder ratio of 1:1 (w/v). The mixture of the two components was stirred with a spatula until a homogeneous paste was formed. The paste was then left to harden at room temperature. The result is called the HASiO₂_PE composite or CPC.

Characterizations

The Fourier Transform-Infrared spectrophotometer (FTIR, Shimadzu Prestige 21) was used to identify functional groups through a KBr pellets method. The X-Ray Diffractometer (XRD, Shimadzu type XRD-6000) equipped with monochromatic Cu K α radiation operated at 40 kW ($\lambda = 1.54 \text{ \AA}$) was used to characterize the crystal structure. The X-ray scanned in the range of $3^\circ \leq 2\theta \leq 80^\circ$ with a scan step degree of 0.02° . The XRD data was analyzed through Rietveld refinement by MAUD 2.933 software. The standard Crystallography Information File (CIF) for HA (COD-1011242) was obtained from the Crystallography Open Database (COD) website. Surface morphology and element distribution were observed using Scanning Electron Microscope-Energy Dispersive Spectroscopy (SEM-EDS, Hitachi type SU3500) and JEOL (type JED-2300) for HASiO₂ and HASiO₂_PE, respectively. Hitachi MC1000 sputter ion was used for sample coating with gold in a thickness of 1 nm. Surface area analysis was conducted by BET method using Quantachrome Instruments version 11.03.

Antibacterial activity was tested by using the diffuse method using *E. coli* (gram-negative) and *S. aureus* (gram-positive) bacteria. The concentrations of *E. coli* and *S. aureus* were 2.6×10^6 and 1.8×10^6 CFU/mL, respectively. The sample concentration was produced by dissolving 0.5 g HASiO₂_PE in 5 mL DMSO. The test was carried out on a Nutrient Agar medium, with a petri dish size of 12 cm, and incubation at 37 °C.

Cytotoxicity test was conducted using pre-osteoblast MC3T3E1 cells grown in MEM- α media, supplemented with 10% FBS, 2% Pen-Strep, and Fungizone 0.5%. Cells were cultivated in 96-well plates. In each well, 100 μ L of cell suspension (contain 2×10^4 cells)

was incubated for 24 h. Then it was treated with HASiO₂_PE according to the serial concentration and incubated for 24 h. The MTT assay was performed by injecting 100 μ L of 0.5 mg/mL MTT into each well, incubated for 4 h, and stopped with DMSO 100 μ L/well. The absorbance was measured using Tecan Spark® (Tecan Trading AG, Switzerland) at 570 nm. Calculation of IC₅₀ values was done by non-linear regression using GraphPad Prism 7 software. The average value of cell viability with HASiO₂_PE treatment was calculated by Microsoft Excel and One Way ANOVA with GraphPad Prism 7 software (GraphPad Software, CA, USA). The cell viability was calculated by:

$$\% \text{Viability} = \frac{\text{OD treatment} - \text{OD media control}}{\text{OD cell control} - \text{OD media control}} \times 100\%$$

RESULTS AND DISCUSSION

Mixing the powder and liquid components using a spatula produced a homogeneous CPC paste. The time needed to form the paste was about 2 min, and the time needed for the paste to harden into cement was about 3 h (Fig. 1). The characterization with FTIR for HASiO₂, PE, and the HASiO₂_PE composite is shown in Fig. 2. In the PE spectra, it can be seen that the specific peaks have the aromatic C=C functional group (1600 cm^{-1}), the -OH phenolic functional group (3450 cm^{-1}) and the C-O-C ether functional group (1166 cm^{-1}). The HASiO₂ spectra identified functional groups that are identical to HA. The presence of PO₄³⁻ group is identified by asymmetric stretching (ν_3) that appears as sharp peaks at 1088 and 1043 cm^{-1} , and asymmetric deformation (ν_4) at 568 and 604 cm^{-1} [24-25]. The O-H group of HA and the adsorbed H₂O appear as broad peaks around 3500 cm^{-1} .



Fig 1. Paste (left) and cement (right) of HASiO₂_PE composite

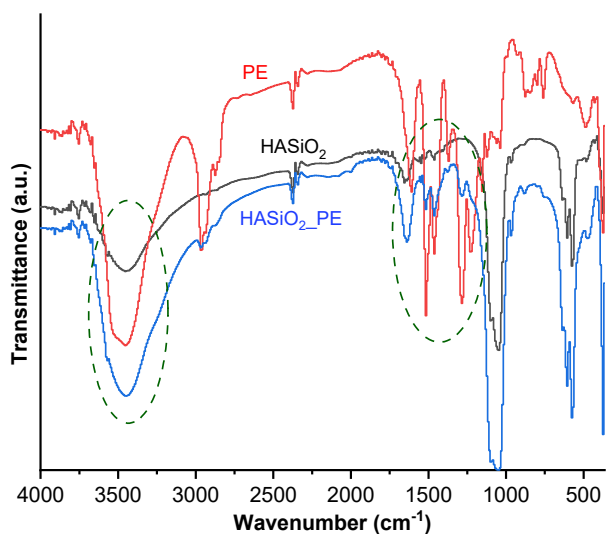


Fig 2. FTIR spectra of HASiO₂, PE, and HASiO₂_PE

A peak at 1637 cm⁻¹ ensures the presence of adsorbed H₂O. Some of PO₄³⁻ in the HA structure were substituted by CO₃²⁻ groups due to the presence of a peak at 1489 cm⁻¹. The Si–O–Si asymmetric stretching vibration coincides with the PO₄³⁻ asymmetric stretching vibration peak at 1088 cm⁻¹ [11]. The HASiO₂ and PE spectral patterns were found in the HASiO₂_PE spectra, but the peak intensity of PE in HASiO₂_PE is lower than HASiO₂ due to its low concentration (10%).

The XRD diffractogram (Fig. 3) shows that PE is amorphous due to the wide peak at 2θ = 5–30°. The diffraction patterns of HASiO₂ and HASiO₂_PE composites are very similar, except for 2θ = 5–25°, in which HASiO₂_PE composite has a higher intensity. HA lattice crystal is known as hexagonal with a space group P63/m. The Rietveld refinement using MAUD 2.993 software showed no change in the lattice parameters of HA due to the composite formation (Fig. 4). Lattice parameters of HA in HASiO₂ and HASiO₂_PE are a = b = 9.47 Å, c = 6.92 Å, and lattice volume = 537.4 Å³. The crystallite sizes of HA in HASiO₂ and HASiO₂_PE are 14.56 and 14.49 nm, respectively (Table 1). These results

are similar to previous studies and COD-1011242 as the standard [26-27]. The same lattice parameters of HA and the same crystallite size of HASiO₂ and HASiO₂_PE are highly expected because HA's bioactivity depends on its lattice parameters. The bioactivity of HA is determined by its solubility properties, where the solubility of solids is determined by its crystal parameters. The similarity of HASiO₂_PE crystallite size with bone mineral size (> 40 nm) supports its compatibility with bone tissue [6].

The BET method determined surface area, pore volume, and pore average. Fig. 5 shows the isotherm graphs for HASiO₂ and HASiO₂_PE. Both samples demonstrated a type III adsorption-desorption isotherm curve, where the adsorbent quantity rose as the relative pressure increased. The adsorbate-adsorbate interaction is stronger than the adsorbent-adsorbent. Type III has an unlimited number of layers on the surface of the adsorbent (multilayer). The decrease in the vertical axis is caused by the fact that the amount of N₂ absorbed by the composite reduces by decreasing pressure. A standard BET multi-point was used to calculate the

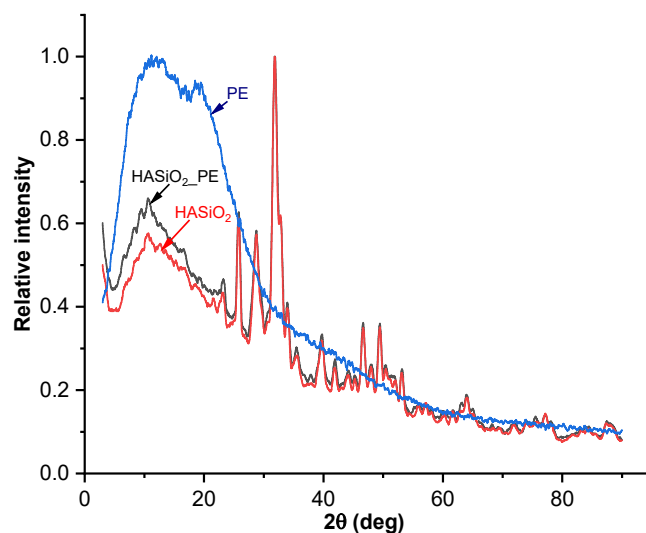


Fig 3. XRD diffractogram

Table 1. Crystal lattice parameters

Sample	a (Å)	c (Å)	Volume (Å ³)	Crystallite size (nm)	Rietveld agreement factors	
					χ ²	Rw (%)
HASiO ₂	9.47	6.92	537.4	14.56	1.31	10.56
HASiO ₂ _PE	9.47	6.92	537.4	14.49	1.30	10.27

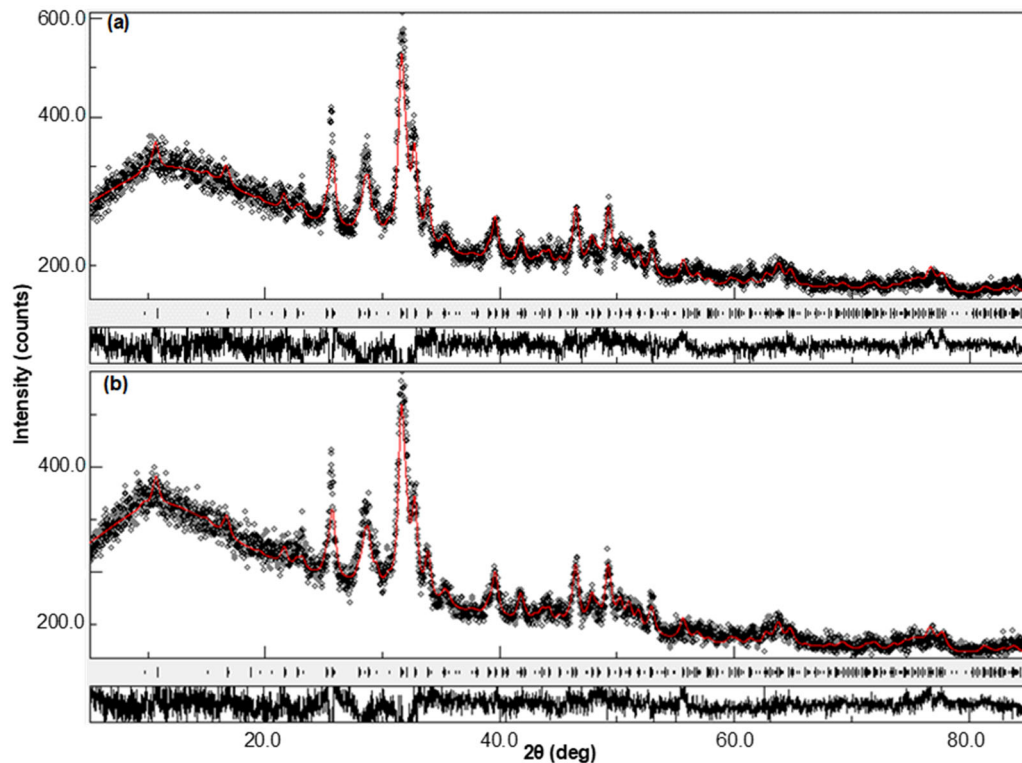


Fig 4. Results of refinement for (a) HASiO₂ and (b) HASiO₂_PE

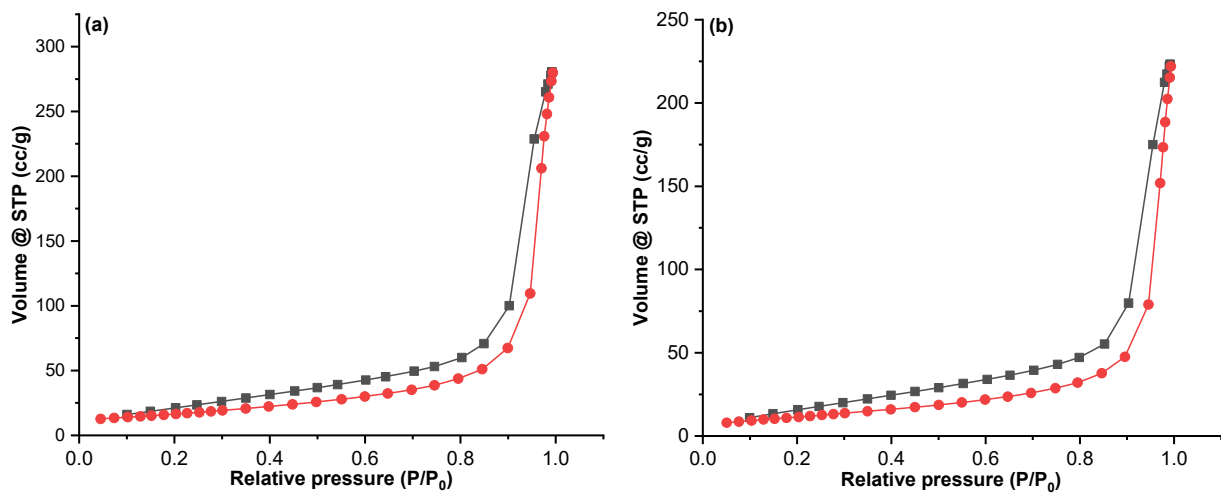


Fig 5. Graph of (a) HASiO₂ and (b) HASiO₂_PE isotherms

specific surface area of the two materials.

HA structure modification usually affects the adsorption-desorption behavior, surface area, total pore volume, and average pore size [28–30]. Table 2 shows that HASiO₂ and HASiO₂_PE have a specific surface area of 59.295 and 43.350 m²/g, respectively. HASiO₂ has a larger surface area than the HASiO₂_PE sample, or making composites reduces the surface area by 26.89%. The total

pore volume also decreased from 0.433 to 0.343 (cm³/g). However, the HASiO₂_PE composite has an average pore size larger than HASiO₂, which is 15.844 and 14.606 nm, respectively. The pore size is included in the mesoporous category (range of pore size 2–50 nm). Thus, both HASiO₂ and HASiO₂_PE have surface properties that support bone cell attachment and proliferation.

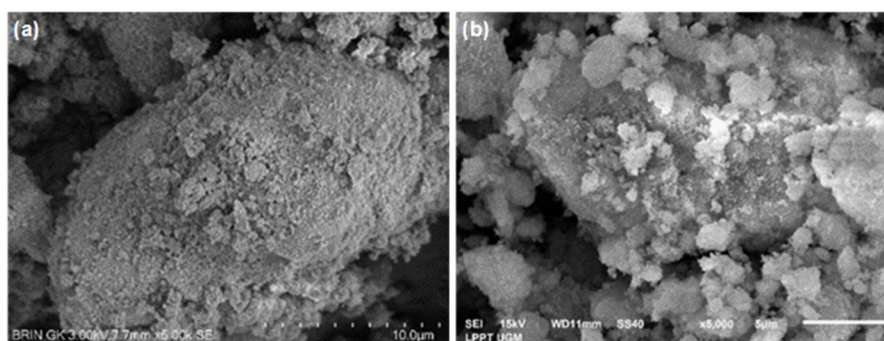
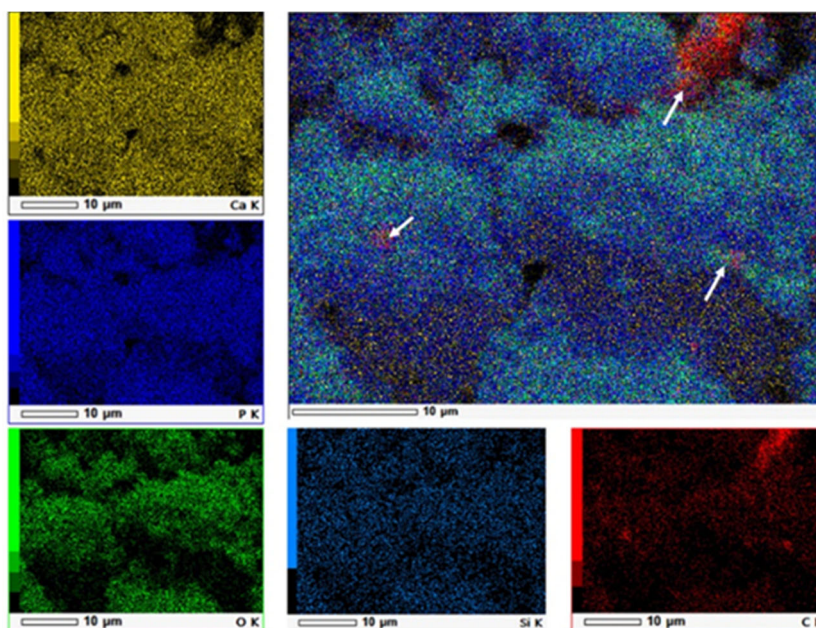
Table 2. Comparison of surface area, pore volume and pore average

Sample	Surface area (S_{BET}) (m^2/g)	Total pore volume (V_{TOT}) (cm^3/g)	Average pore size (nm)
HASiO ₂	59.295	0.433	14.606
HASiO ₂ _PE 10%	43.350	0.343	15.844

The analysis results with SEM at 5000 times magnification showed that the surface morphology of HASiO₂ is uneven (Fig. 6). The agglomeration of nano-sized particles leads to the formation of a variety of particle sizes. The large particles showed a consistent shape, a capsule-like shape, with dimensions on a micron scale. In the HASiO₂_PE composite, the particle shape is irregular, and the morphology is uneven. The agglomeration behavior of the two samples was different, despite the fact that the XRD data did not show any

difference in the HA lattice parameters and the crystallite size. The surface of the HASiO₂_PE composite is rougher and denser than HASiO₂. Synthesis of HA-modified silica without using CTAB surfactants produced a flat surface, unlike in this study [11].

Element mapping on the surface of the HASiO₂_PE composite has shown how the composite surface is covered by Ca, P, O, Si, and C elements (Fig. 7). The presence of Ca, P, O, and Si elements indicate the presence of HASiO₂, while C and O indicate the presence

**Fig 6.** Surface profiles of (a) HASiO₂ and (b) HASiO₂_PE**Fig 7.** Results of elemental mapping on the HASiO₂_PE surface

of PE. On individual mapping, Ca dominates the composite surface and is evenly distributed. There are several dark areas that are confirmed as C elements (from PE). The same distribution pattern occurs for the P element mapping. The P elements belong to HA, where Ca^{2+} binds to PO_4^{3-} through Ca-O-P bonds. The O element shows a slightly different pattern, in which O forms a contour that can be compared with the combined element mapping results. It can be concluded that O tends to be found on the composite surface or is exposed on the surface. This is highly desirable because the presence of O, mainly in the form of phosphate, carbonate, or hydroxyl groups, supports the biocompatibility and bioactivity of the composite in physiological environments [28]. The distribution of Si elements has the same pattern as Ca and P elements. Confirming the results of earlier research that the silica-modified HA composite had silica within and HA on the surface [11]. C Element appears to be partially distributed and agglomerated in some areas, filling in the dark areas on the mapping of Ca and P elements. This confirmed that the hydrophobicity of PE is high so that PE is not soluble in the Na_2HPO_4 solution. The combined mapping showed that the composite surface is uneven and that the PE (arrows) agglomerates on some of the surface's area. Such a surface supports the attachment of cells and ions when the composite is in a physiological environment [29].

The elemental composition on the surface was measured by EDX and the results could be seen in Table 3. Compositing HAsiO_2 and PE caused the amount of Ca to decrease significantly from 33.00 to 13.00%. This is because C, which represents the presence of PE, covers the surface in a large amount, namely 20%. This also causes a decrease in the P element from 11.40 to 9.00%. On the other hand, the amount of O element experienced a slight increase from 54.80 to 57.70%, which was a contribution from PE. The same with Ca and P, the amount of Si decreases from 0.80 to 0.30%. This condition caused the Ca/P ratio to decrease from 2.89 to 1.44, indicating that Ca no longer dominates the surface compared to P. This also causes the Ca/O ratio to decrease, in addition to the increase in the amount of O element on the surface. The presence of PE on the surface is expected

Table 3. Elemental composition on the surface of HAsiO_2 and $\text{HAsiO}_2\text{-PE}$

Element	Atomic (%)	
	HAsiO_2	$\text{HAsiO}_2\text{-PE}$
Ca	33.00	13.00
P	11.40	9.00
O	54.80	57.70
Si	0.80	0.30
C	-	20.00
Ca/P	2.89	1.44
Ca/O	0.60	0.23

Table 4. Antibacterial test results

Sample	<i>E. coli</i>		<i>S. aureus</i>	
	Inhibition zone (mm)	Average (mm)	Inhibition zone (mm)	Average (mm)
PE	1.60	1.80	2.00	2.30
	1.90		2.60	
	1.90		2.30	
$\text{HAsiO}_2\text{-PE}$	3.10	2.83	1.50	1.43
	2.50		1.40	
	2.90		1.40	
Chloramphenicol	11.00	11.50	13.20	14.00
	12.00		14.90	
	11.50		13.90	
Erythromycin	5.40	5.97	5.40	5.07
	6.30		5.30	
	6.20		4.50	

because PE will interact directly with the physiological environment, and the degradation of PE from the cement will bring about the antibacterial activity. The presence of PE on the surface did not reduce the hydrophilicity of HASiO₂ according to the surface wetting test. As a result, the HASiO₂_PE composite retains the superior properties of HA.

The antibacterial test was carried out using *E. coli* and *S. aureus* bacteria. The inhibition zone of PE and HASiO₂_PE compared to chloramphenicol and erythromycin is shown in Table 4. PE has better antibacterial activity against *S. aureus* than *E. coli*. This result is different from the previous research that found PE to have the same activity against both bacteria [31]. In contrast, the HASiO₂_PE composite revealed better antibacterial activity on *E. coli* than *S. aureus*. This could

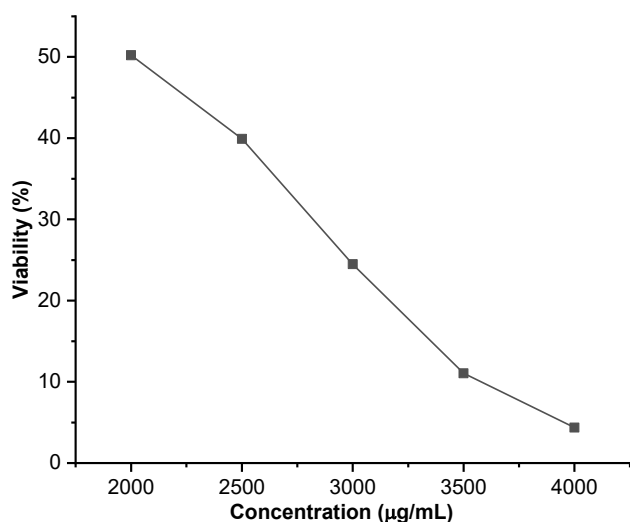


Fig 8. Graph of pre-osteoblast cell viability at various concentrations of the HASiO₂_PE composite

be due to the synergy of HASiO₂ and PE has produced a higher antibacterial activity toward a gram-negative than a gram-positive bacterium. It may also be due to the small amount of PE (10%) compared to HASiO₂. The antibacterial activity toward *S. aureus* can be increased by increasing the PE content in the composite.

The cytotoxicity test of HASiO₂_PE composite was conducted by MTT assays with an incubation time of 24 h using *pre-osteoblast* cells. Percent viability decreased non-linearly with the concentration of HASiO₂_PE (Fig. 8). The calculation obtained the IC₅₀ value = 2092 µg/mL with R² = 0.9446. These data indicate that the HASiO₂_PE composite is non-toxic or biocompatible and can be accepted by bone cells [32-33]. A comparison of the cells' state in control and in the 2000 µg/mL of HASiO₂_PE resulted in the different numbers of cells or cell population (Fig. 9). Some cells seem to change in shape and size, the shape changes to round, and the size becomes smaller. Based on the IC₅₀ value and the cell morphology profile, it is feasible to conclude that the CPC made from the HASiO₂_PE composite is biocompatible [12]. The composite will promote osteoblast proliferation and is predicted to play positive roles in osteoblast differentiation and next to the mineralized bone matrix formation [34-35].

CONCLUSION

Compositing 10% (w/w) PE and HASiO₂ did not affect the HA crystal structure in which the lattice parameters are counted as a = b = 9.47 Å, c = 6.92 Å, and lattice volume = 5374 Å³. The HA crystallite size is close to bone mineral size (> 40 nm). The composite has a

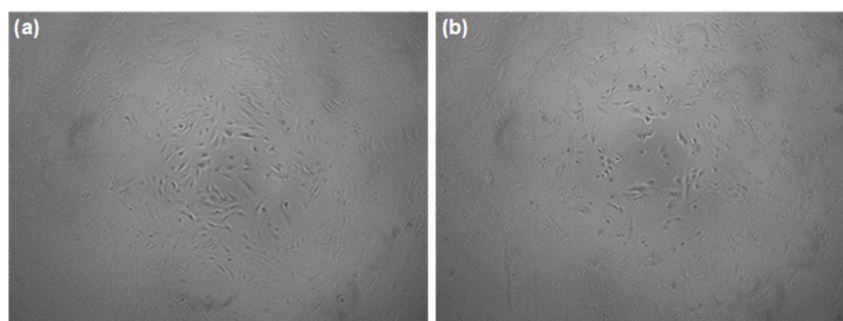


Fig 9. Morphological differences between (a) control cells and (b) HASiO₂_PE 2000 µg/mL in the cytotoxicity test with the MTT assay

morphology that is coarser and denser than HASiO₂. PE that contributes antibacterial activity can be found on the composite's surface. Both HASiO₂ and the composite have a relatively similar surface area, total pore volume, and average pore size. Compositing PE with HASiO₂ decreased its antibacterial activity toward *S. aureus* but increased its antibacterial activity against *E. coli*. The composite is non-toxic due to the IC₅₀ of 2092 µg/mL when tested with pre-osteoblast cells. As long as the non-toxic property can be maintained, increasing the PE content in the composite is recommended to boost the antibacterial activity toward *S. aureus*.

■ ACKNOWLEDGMENTS

The authors gratefully acknowledge Faculty of Mathematics and Sciences, Universitas Diponegoro, Semarang, Indonesia for the financial support through the research grant "Riset Madya" with the contract number: 1263J/UN7.5.8/PP/2022.

■ AUTHOR CONTRIBUTIONS

Tri Windarti, Nor Basid Adiwibawa Prasetya, and Ngadiwiyana carried out the experiment, Limpat Nulandaya carried out the refinement of XRD data, all authors analyzed data and wrote the manuscript.

■ REFERENCES

- [1] Flurin, L., Greenwood-Quaintance, K.E., and Patel, R., 2019, Microbiology of polymicrobial prosthetic joint infection, *Diagn. Microbiol. Infect. Dis.*, 94 (3), 255–259.
- [2] Tubb, C.C., Polkowksi, G.G., and Krause, B., 2020, Diagnosis and prevention of periprosthetic joint infections, *J. Am. Acad. Orthop. Surg.*, 28 (8), e340–e348.
- [3] Izakovicova, P., Borens, O., and Trampuz, A., 2019, Periprosthetic joint infection: Current concepts and outlook, *EFORT Open Rev.*, 4 (7), 482–494.
- [4] Lipsky, B.A., Weigelt, J.A., Gupta, V., Killian, A., and Peng, M.M., 2007, Skin, soft tissue, bone, and joint infections in hospitalized patients: Epidemiology and microbiological, clinical, and economic outcomes, *Infect. Control Hosp. Epidemiol.*, 28 (11), 1290–1298.
- [5] Maaloum, Y., Meybeck, A., Olive, D., Boussekey, N., Delannoy, P.Y., Chiche, A., Georges, H., Beltrand, E., Senneville, E., d'Escrivan, T., and Leroy, O., 2013, Clinical spectrum and outcome of critically ill patients suffering from prosthetic joint infections, *Infection*, 41 (2), 493–501.
- [6] Ginebra, M.P., Espanol, M., Montufar, E.B., Perez, R.A., and Mestres, G., 2010, New processing approaches in calcium phosphate cements and their applications in regenerative medicine, *Acta Biomater.*, 6 (8), 2863–2873.
- [7] Akao, M., Aoki, H., and Kato, K., 1981, Mechanical properties of sintered hydroxyapatite for prosthetic applications, *J. Mater. Sci.*, 16 (3), 809–812.
- [8] Moheet, I.A., Luddin, N., Ab Rahman, I., Masudi, M., Kannan, T.P., and Nik Abd Ghani, N.R., 2018, Evaluation of mechanical properties and bond strength of nano-hydroxyapatite-silica added glass ionomer cement, *Ceram. Int.*, 44 (8), 9899–9906.
- [9] Villacampa, A.I., and García-Ruiz, J.M., 2000, Synthesis of a new hydroxyapatite-silica composite material, *J. Cryst. Growth*, 211 (1), 111–115.
- [10] Lei, C., Cao, Y., Hosseinpour, S., Gao, F., Liu, J., Fu, J., Staples, R., Ivanovski, S., and Xu, C., 2021, Hierarchical dual-porous hydroxyapatite doped dendritic mesoporous silica nanoparticles based scaffolds promote osteogenesis *in vitro* and *in vivo*, *Nano Res.*, 14 (3), 770–777.
- [11] Windarti, T., Widjijono, W., and Nuryono, N., 2021, Deposition of hydroxyapatite on silica made from rice husk ash to produce powder component of calcium phosphate cement, *Indones. J. Chem.*, 21 (3), 588–597.
- [12] Qiao, Y., Zhai, Z., Chen, L., and Liu, H., 2015, Cytocompatible 3D chitosan/hydroxyapatite composites endowed with antibacterial properties: toward a self-sterilized bone tissue engineering scaffold, *Sci. Bull.*, 60 (13), 1193–1202.
- [13] Yang, Y., Campbell Ritchie, N., and Everitt, N.M., 2021, Recombinant human collagen/chitosan-based soft hydrogels as biomaterials for soft tissue engineering, *Mater. Sci. Eng., C*, 121, 111846.

- [14] Shu, X., Liao, J., Wang, L., Shi, Q., and Xie, X., 2020, Osteogenic, angiogenic, and antibacterial bioactive nano-hydroxyapatite co-synthesized using γ -polyglutamic acid and copper, *ACS Biomater. Sci. Eng.*, 6 (4), 1920–1930.
- [15] Li, Z., Zhou, P., Zhou, F., Zhao, Y., Ren, L., and Yuan, X., 2018, Antimicrobial eugenol-loaded electrospun membranes of poly(ϵ -caprolactone)/gelatin incorporated with REDV for vascular graft applications, *Colloids Surf., B*, 162, 335–344.
- [16] Modjinou, T., Versace, D.L., Abbad-Andaloussi, S., Langlois, V., and Renard, E., 2017, Antibacterial and antioxidant photoinitiated epoxy co-networks of resorcinol and eugenol derivatives, *Mater. Today Commun.*, 12, 19–28.
- [17] Li, M., Yu, H., Xie, Y., Guo, Y., Cheng, Y., Qian, H., and Yao, W., 2021, Fabrication of eugenol loaded gelatin nanofibers by electrospinning technique as active packaging material, *LWT*, 139, 110800.
- [18] Xu, H., Zhang, D., and Li, J., 2019, Antibacterial nanoparticles with universal adhesion function based on dopamine and eugenol, *J. Bioresour. Bioprod.*, 4 (3), 177–182.
- [19] Melendez-Rodriguez, B., Figueroa-Lopez, K.J., Bernardos, A., Martínez-Máñez, R., Cabedo, L., Torres-Giner, S., and Lagaron, J.M., 2019, Electrospun antimicrobial films of poly(3-hydroxybutyrate-co-3-hydroxyvalerate) containing eugenol essential oil encapsulated in mesoporous silica nanoparticles, *Nanomaterials*, 9 (2), 227.
- [20] Saltan, F., 2021, Preparation of poly(eugenol-co-methyl methacrylate)/polypropylene blend by creative route approach: Structural and thermal characterization, *Iran. Polym. J.*, 30 (11), 1227–1236.
- [21] Predoi, S.A., Ciobanu, C.S., Motelica-Heino, M., Chifiriuc, M.C., Badea, M.L., and Iconaru, S.L., 2021, Preparation of porous hydroxyapatite using cetyl trimethyl ammonium bromide as surfactant for the removal of lead ions from aquatic solutions, *Polymers*, 13 (10), 1617.
- [22] Li, Y., Tjandra, W., and Tam, K.C., 2008, Synthesis and characterization of nanoporous hydroxyapatite using cationic surfactants as templates, *Mater. Res. Bull.*, 43 (8-9), 2318–2326.
- [23] Larsson, S., Stadelmann, V.A., Arnoldi, J., Behrens, M., Hess, B., Procter, P., Murphy, M., and Pioletti, D.P., 2012, Injectable calcium phosphate cement for augmentation around cancellous bone screws. In vivo biomechanical studies, *J. Biomech.*, 45 (7), 1156–1160.
- [24] Fahami, A., Beall, G.W., and Betancourt, T., 2016, Synthesis, bioactivity and zeta potential investigations of chlorine and fluorine substituted hydroxyapatite, *Mater. Sci. Eng., C*, 59, 78–85.
- [25] Malakauskaite-Petruleviciene, M., Stankeviciute, Z., Niaura, G., Prichodko, A., and Kareiva, V., 2015, Synthesis and characterization of sol-gel derived calcium hydroxyapatite thin films spin-coated on silicon substrate, *Ceram. Int.*, 41 (6), 7421–7428.
- [26] da Silva Brum, I., de Carvalho, I.I., da Silva Pires, J.L., de Carvalho, M.A.A., dos Santos, L.B.F., and Elias, C.N., 2019, Nanosized hydroxyapatite and β -tricalcium phosphate composite: Physico-chemical, cytotoxicity, morphological properties and *in vivo* trial, *Sci. Rep.*, 9 (1), 19602.
- [27] Singh, G., Jolly, S.S., and Singh, R.P., 2020, Cerium substituted hydroxyapatite mesoporous nanorods: Synthesis and characterization for drug delivery applications, *Mater. Today: Proc.*, 28, 1460–1466.
- [28] Wilson, O.C., and Hull, J.R., 2008, Surface modification of nanophase hydroxyapatite with chitosan, *Mater. Sci. Eng., C*, 28, 434–437.
- [29] Fuh, L.J., Huang, Y.J., Chen, W.C., and Lin, D.J., 2017, Preparation of micro-porous bioceramic containing silicon-substituted hydroxyapatite and beta-tricalcium phosphate, *Mater. Sci. Eng., C*, 75, 798–806.
- [30] Hajimirzaee, S., Chansai, S., Hardacre, C., Banks, C.E., and Doyle, A.M., 2019, Effects of surfactant on morphology, chemical properties and catalytic activity of hydroxyapatite, *J. Solid State Chem.*, 276, 345–351.
- [31] Prasetya, N.B.A., Asiyah, A., Sarjono, P.R., Ngadiwiyana, N., and Ismiyanto, I., 2021, Synthesis

- of sulfonated poly-(eugenol divinylbenzene) nanosilver composite and its application as antibacterial compound of cotton fabric, *J. Phys.: Conf. Ser.*, 1943, 012183.
- [32] Baharum, Z., Akim, A.M., Taufiq-Yap, Y.H., Hamid, R.A., and Kasran, R., 2014, *In vitro* antioxidant and antiproliferative activities of methanolic plant part extracts of *Theobroma cacao*, *Molecules*, 19 (11), 18317–18331.
- [33] Atjanasuppat, K., Wongkham, W., Meepowpan, P., Kittakooop, P., Sobhon, P., Bartlett, A., and Whitfield, P.J., 2009, *In vitro* screening for anthelmintic and antitumour activity of ethnomedicinal plants from Thailand, *J. Ethnopharmacol.*, 123 (3), 475–482.
- [34] Noor, M., Al Mamun, M.A., Atique Ullah, A.K.M., Matsuda, A., Kawamura, G., Hakim, M.A., Islam, M.F., and Matin, M.A., 2021, Physics of $Ce^{3+} \leftrightarrow Ce^{4+}$ electronic transition in phytosynthesized $CeO_2/CePO_4$ nanocomposites and its antibacterial activities, *J. Phys. Chem. Solids*, 148, 109751.
- [35] Liu, J.L., Zhang, B., Song, S.J., Ma, M., Si, S.Y., Wang, Y.H., Xu, B.X., Feng, K., Wu, J.G., and Guo, Y.C., 2014, Bovine collagen peptides compounds promote the proliferation and differentiation of MC3T3-E1 pre-osteoblasts, *PLoS One*, 9 (6), e99920.